An experimental and theoretical study of ring closing dynamics in HN_3

Jianyang Zhang,[ab] Peng Zhang,[c] Yuan Chen,[a] Kaijun Yuan,[a] Steven A. Harich,[a] Xiuyan Wang,[ab] Zhi Wang,[c] Xueming Yang,[a] Keiji Morokuma[c] and Alec M. Wodtke*[d]

Received 16th January 2006, Accepted 17th February 2006
First published as an Advance Article on the web 1st March 2006
DOI: 10.1039/b600599c

We report on an H(D)-atom Rydberg tagging experiment for $H(D)N_3$ photolysis providing detailed dynamical information on the wavelength dependence of the $H(D) + N_3$ channel. We observe subtle yet striking changes in the photochemical dynamics as the photolysis energy passes through ~5.6 eV. In addition to producing linear azide with an average of ~40% of available energy appearing as translation, a second H(D)-atom producing channel grows in above this energy releasing only about 15%. An observed (inverse) isotope effect suggests that statistical decomposition on S_0 is unimportant. High level *ab initio* quantum chemical calculations reveal a transition state to cyclization of the N_3 moiety in $H(D)N_3$ on the first excited singlet (S_1) surface that is close in energy to the experimentally observed threshold energy for this "slow channel". Furthermore, the translational energy release of the "slow channel" is energetically consistent with cyclic-N_3 formation. This work provides the clearest presently available insights into how ring closure can occur in azide photochemistry.

Introduction

While a large number of all-nitrogen species have been predicted theoretically,[1–6] there are to date only five allotropes of nitrogen that have been identified experimentally,[7,8] three of which are N_2, N_3 and N_3^-. One of the fundamental barriers to exploring the full diversity of all-nitrogen molecules is their near pathological resistance to ring formation. Experimental schemes that could demonstrate ring formation would provide new possibilities to the expansion of this intriguing field of chemistry. For some time, one of us (AMW) has proposed that cyclic-N species might be produced from suitable photochemical precursors. Several recent experiments[9–14] provide evidence that the UV photolysis of ClN_3 leads efficiently to the simplest cyclic all-nitrogen allotrope, cyclic-N_3.[15–18]

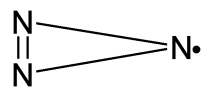

These results stand, however, in stark contrast to the paucity of theoretical studies on ClN_3 photochemistry and consequently, the photochemical mechanism remains unclear as to which azides may undergo photochemical ring-closure. In the hopes of perhaps finding another example of photochemical production of cyclic-N_3 and more importantly one where high-level quantum chemical methods could be used to guide our analysis of the microscopic reaction mechanism, we undertook a study of the photochemistry of hydrazoic acid, HN_3, the simplest member of the XN_3 family.

The UV photochemistry of HN_3 (especially in its first excited singlet state, S_1, possessing A″ symmetry) has attracted much attention; one might even refer to it as a benchmark system for the study of polyatomic ultraviolet photochemical dynamics. All four of the products of HN_3 photolysis:

$$HN_3 \rightarrow H + N_3 \; \Delta E = 88.7 \text{ kcal mol}^{-1} \text{ - Channel} \quad (1)$$

$$\rightarrow NH(a^1\Delta) + N_2 \; \Delta E = 63.5 \text{ kcal mol}^{-1} \text{ - Channel} \quad (2)$$

are suitable for efficient detection by optical means, thus the reaction has been studied with several quantum-state resolved methods.[19–37] HN_3 is also particularly amenable to high level *ab initio* quantum chemistry methods in both ground and excited electronic states,[38–40] making comparison between experiment and theory particularly useful for the analysis of its photochemistry.

It is noteworthy that the possible formation of cyclic-N_3 in HN_3 photochemistry has never been the focus of any of these many high quality studies. Channel (2), which dominates at photolysis wavelengths where branching ratios have been measured,[29] has attracted much of the attention.[19–26] Of those experiments focused on channel (1),[27–32] most employed photolysis wavelengths where cyclic-N_3 was not energetically accessible, $\lambda > 244$ nm, or employed methods that would not reveal the production of this molecule.

The H-atom Rydberg time-of-flight (HRTOF)[41] method is one of the few possible means by which the formation of cyclic-N_3 in HN_3 photolysis might be observed and studied. Furthermore, it has already proven useful in understanding the dynamics of channel (1).[27,28] Cook *et al.* reported HRTOF

[a] *State Key Laboratory for Molecular Dynamics, Dalian Institute of Chemical Physics, 457 Zhongshan Rd. Dalian, Liaoning, 116023, P. R. China*
[b] *Department of Physics, Dalian University of Technology, Dalian, China*
[c] *Cherry L. Emerson Center for Scientific Computation and Department of Chemistry, Emory University, Atlanta, Georgia, 30322, USA*
[d] *Department of Chemistry and Biochemistry, University of California, Santa Barbara, CA 93106-9510, USA. E-mail: wodtke@chem.ucsb.edu*

results for photolysis wavelengths between 240 and 280 nm, providing comprehensive characterization of the energy release to photoproducts after excitation to the S_1 state.[28] Also demonstrating the power of comparison between experiment and theory for this system, analysis with an *ab initio* potential energy surface using wave packet calculations helped support the vibrational assignment of the well resolved features in the HRTOF energy distribution.[39] This work produced no evidence of cyclic-N_3 formation despite the fact that some of the reported photolysis wavelengths surpassed its energetic formation threshold.[42] Zhang *et al*. are the only group to report HRTOF results on HN_3 at shorter wavelengths still; they carried out photolysis experiments at 248 and 193 nm.[27] While these results do not reveal the full nature of the wavelength dependence of channel (1), photolysis at 193-nm clearly leads to more internally excited N_3 molecules than does photolysis at all other wavelengths that have been studied.[27] This suggested to us the value of a more comprehensive and systematic study of the wavelength dependent dynamics of photochemical H-production in HN_3.

Recently, we have completed such a study using the HRTOF method, spanning the range of photolysis wavelengths between 280 and 188 nm in roughly 5 nm steps. A full analysis of these results will be reported later. This paper focuses on the 5–6 eV energy range (225–199 nm), where a marked transition in the photochemical dynamics is observed. We observe many of the same features seen previously corresponding to formation of linear azide, where on average 40% of the available energy is channeled to translation. In addition, these results reveal a low-translational-energy, H-atom producing channel that grows in importance above a threshold of $\sim$5.6 eV. The translational energy release of this "slow component" is consistent with known thermodynamics for formation of cyclic-N_3 Furthermore, a comparison to high level *ab initio* quantum chemistry calculations reveals that the experimentally observed threshold for this channel is coincident with an N_3-ring closing transition state for HN_3 on its S_1 potential energy surface that leads to an electronically excited cyclic intermediate of HN_3. Theory shows that this intermediate may dissociate over a small barrier to H + cyclic-N_3. These results provide the first insight into the microscopic mechanism for N_3 ring closure in XN_3 photochemistry.

Methodology

We used a multidisciplinary methodology to approach this problem combining high level HRTOF experiments with the best available quantum chemistry methods.

Experiment

The H/D-Rydberg-atom-time-of-flight (HRTOF) technique has been described in detail elsewhere[43,44] and only a brief description of the more salient points is presented here. A skimmed, pulsed, molecular beam of HN_3, seeded in helium (mixing ratio $\sim$2%, total pressure $\sim$1 atm), is crossed at 90° with the output of the photolysis laser (UV power 0.1–4 mJ, with the beam diameter $\geq$ 0.1 cm), which consists of Nd:YAG (Spectra Physics Pro-290) 3rd harmonic pumped dye laser (Sirah, PESC-G-24) system. The second harmonic of the dye laser light is generated using a BBO crystal (tunable in the range of 225–280 nm). Photons in the range of 188 to 225 nm are generated by combining the output of the second harmonic of the dye laser with the Nd:YAG fundamental (1064 nm), using a second BBO crystal. Distributions of recoiling H/D atoms are probed using a detector positioned at different lab angles. After a short time delay ($\sim$10 ns) recoiling H-atom products from the photodissociation were tagged by excitation to high-n Rydberg levels using a two color scheme: Lyman-α radiation at 121.6 nm followed by UV radiation at $\sim$366 nm. Photons at the Lyman-α wavelength are generated by four-wave mixing of two 212.5 nm photons and one 845 nm photon in a cell filled with a 3 : 1 ratio Ar–Kr mixture of at a total pressure about 70 Torr. Photons at 212.5 nm are produced by doubling the output of a Nd:YAG (Spectra Physics Pro-290) 3rd harmonic pumped dye laser (Sirah, PESC-G-24) operating at $\sim$425 nm. A portion of the 532 nm output of the YAG is used to pump another dye laser (Continuum ND6000) operating at $\sim$845 nm. These beams are then focused into a cell with Kr/Ar mixing gas where four wave mixing at 121.6 nm is generated. The remainder of the 532 nm source is used to pump a third Radiant dye laser (Radiant Dye Lasers- Jaguar, D90MA), operating at $\sim$732 nm, the output from which frequency is doubled to $\sim$366 nm, and used to promote the H-atoms from the n = 2 level to a Rydberg state of high principal quantum number (n = 30–90), lying just below the ionization threshold. The beam paths of both tagging lasers have been set to ensure their maximum temporal overlap in the interaction region, and all three beams are focused so as to ensure their maximum mutual spatial overlap within this volume. Any charged species formed at the volume of tagging by initial laser excitation are extracted away from the TOF axis by a small electric field placed across the interaction region.

The tagged H-atoms then fly away from the interaction region to reach a micro-channel plate (MCP) detector. The Rydberg H-atoms are efficiently ionized by the strong electric field applied to the MCP detector. The total distance from the interaction region to the front face of the detector is $\sim$333 mm. The signal obtained is amplified by a preamplifier, discriminated by a discriminator, sent to both a digital oscilloscope for visual display and a multi-channel scaler (P7888-2(E) FASTCOMTEC) for accumulation (typically more than 10^5 laser shots per TOF profile) and subsequent data analysis.

HN_3 was prepared by heating sodium azide (NaN_3) in excess stearic acid under vacuum for 3–4 h at $\sim$80–100 °C. DN_3 was produced by reacting NaN_3 with an excess of deuterated phosphoric acid, which is generated by reacting D_2O with P_2O_5 under vacuum conditions. The $H(D)N_3$ sample was stored in a stainless steel container and He gas was filled to produce 1–2% $H(D)N_3$/He ratio (the total pressure made up to $\sim$1–4 atm with pure helium). Purity was checked by mass spectrometry (SRS, RGA200).

Theory

Geometries of potential energy minima and transition states were optimized using the analytical gradient at the state-specific (ss)-CASSCF (complete active space self-consistent

field) level.[45] In ss-CASSCF calculations, the full valence active space, (16e/13o), consisting of 16 electrons in 13 molecular orbitals, was used with the cc-pVTZ (VTZ), Dunning's correlation consistent polarized valence triple-zeta basis set.[46] The Hessian matrix, vibrational frequencies and the zero point energy (ZPE) were calculated by numerical differentiation of the energy gradient at the same ss-CASSCF/VTZ level as in geometry optimization. Energetics were further refined by the internally contracted configuration interaction with single and double excitations (MRCISD)[47,48] plus multi-reference version of Davidson's correction (Q)[49,50] with the Dunning's correlation consistent augmented polarized valence triple zeta basis (AVTZ),[46] where a pre-determined ss-CASSCF(16e/13o)/AVTZ wave function was selected as the reference configuration. In the MRCISD calculation, only the 1s orbitals of nitrogen atoms were kept doubly occupied in all configurations and the remaining 16 electrons were correlated, denoted as MRCISD(Q)(16e/13o)/AVTZ. MOLPRO 2002.6[51] was used for all the CASSCF and MRCISD calculations.

Results and discussion

Fig. 1 shows the center-of-mass translational energy release distribution for the H(D) + N_3 channel at a few selected photolysis wavelengths obtained by direct inversion of the raw TOF data obtained at the magic recoil angle ($\Theta = 54.7^\circ$) with respect to the original direction of the polarization of the photolysis laser. This angle is useful in that signal intensities are thereby independent of the H-atom angular distribution. In each panel, the isotope (H or D) is indicated as is the photolysis wavelength in nm. For example, D-208 was a D-atom Rydberg tagging experiment at a photolysis wavelength of 208 nm. The downward pointing arrows indicate the thermodynamically-determined limit to the translational

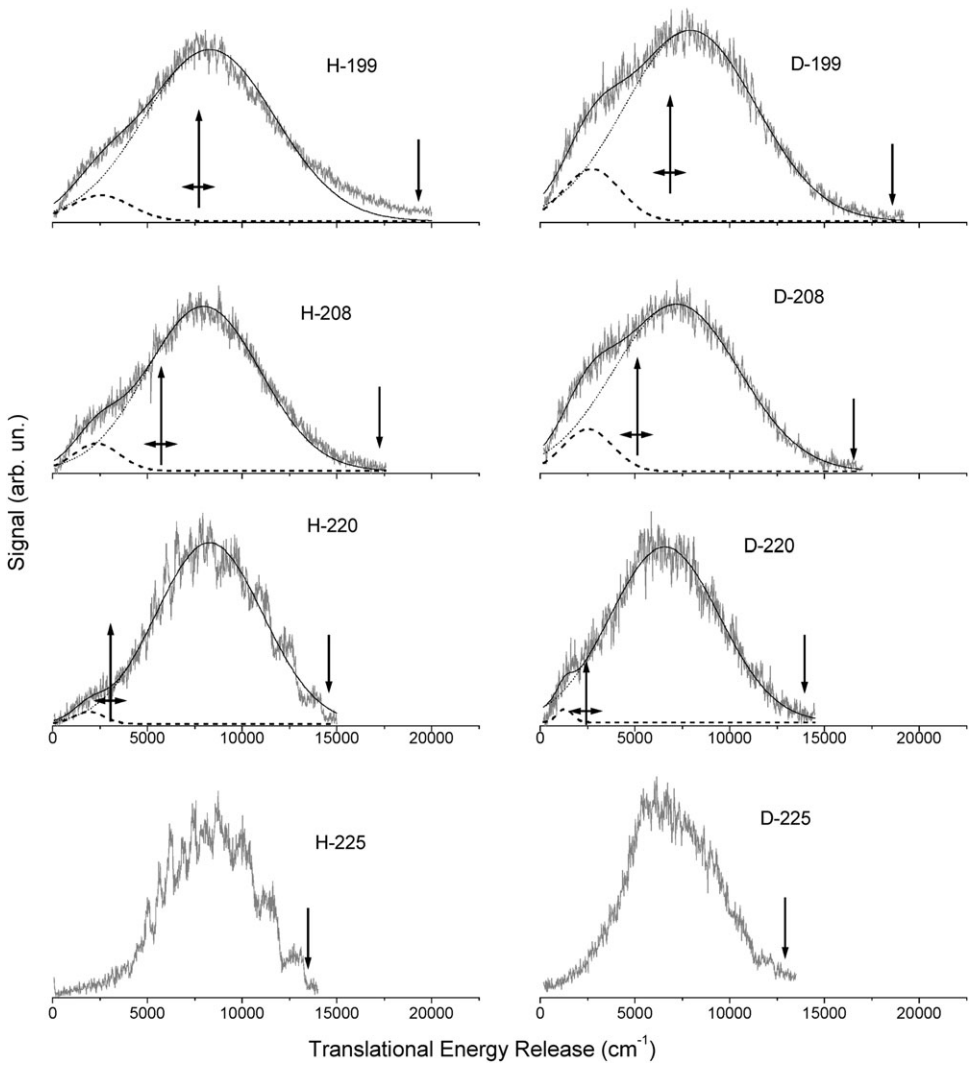

Fig. 1 H-Atom Rydberg TOF derived translational energy release distributions for HN_3 and DN_3 photolysis at representative wavelengths. Two channels are observed at wavelengths shorter than about 220 nm. The low translational energy channel (dashed line) is consistent in energy release with formation of cyclic-N_3, the formation of which cannot lead to translational energies larger than that shown by the upward directed arrows. The high translational energy release channel (dotted line) produces linear-N_3 which has a thermodynamically defined limit to the translational energy release shown by the downward pointing arrows. The double headed arrows represent the uncertainty in our knowledge of the heat of formation of cyclic-N_3. The notation on each panel indicates the isotope (D or H) as well as the photolysis wavelength in nm.

energy release assuming the detected H(D)-atoms are produced with linear N_3-radicals. The partially resolved structure seen in panel H-225 can also be successfully assigned to vibrational states of the linear N_3 -radical as in ref. 27 and 28.

At photolysis wavelengths less than or equal to $\sim$220 nm, a second component to the translational energy release is clearly observable, and is notably stronger for D than for H. This component exhibits a smaller translational energy release, suggesting formation of a form of N_3 with high internal energy. Energy release distributions corresponding to photolysis wavelengths longer than 225 nm qualitatively resemble the 225 nm results and show no sign of this second low-translational-energy component. In order to better quantify the two contributions to the translational energy release distribution, the data was fit to two Gaussian functions, shown as dashed and dotted lines in Fig. 1. One can see that the data is well fit by this simple strategy. The upward pointing arrows (best value) and double-headed horizontal arrow (error bars) show the thermodynamically-determined limit of translational energy release assuming formation of H(D) with cyclic-N_3.[15,16]

The fraction of the H(D)-producing photochemistry that results in the high energy form of N_3 can be estimated by integrating the Gaussian components used to fit the translational energy release distributions of Fig. 1. This is shown for both isotopes in Fig. 2 for photolysis wavelengths: 220, 217, 213, 208, 203 and 199 nm. We found no detectible branching between channels at longer photolysis wavelengths. The observed threshold at a photolysis energy of 5.65 $\pm$ 0.05 eV

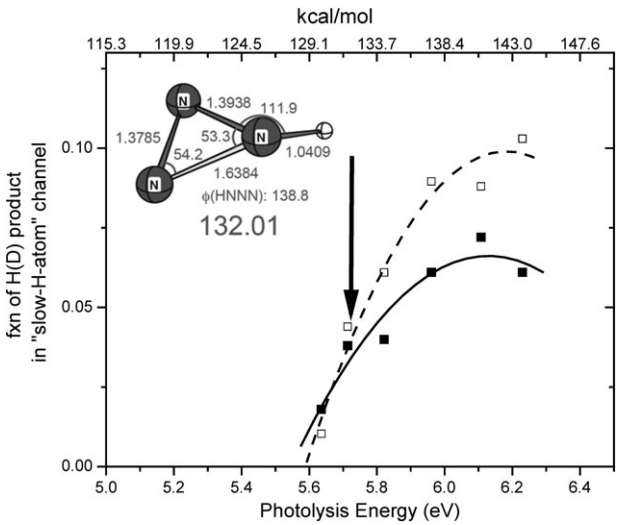

Fig. 2 Observations of barriers in the S_1 state of HN_3. The solid squares show the derived fraction of H-atom channel appearing at low translational energies. This represents the fraction of H-atoms formed together with a *high energy form* of N_3 (possibly cyclic-N_3). The solid arrow shows the theoretically predicted threshold energy for ring-closure on the S_1 surface of HN_3. The accuracy of this prediction is expected to be better than $\pm$0.2 eV. The structure of the calculated transition state to ring closure on the S_1 surface is shown as an inset. This comparison between theory and experiment provides strong evidence for the observation of ring closure in the UV photolysis of HN_3. Open squares show the results of DN_3 photolysis. The isotope effect favoring D-atoms may be indicative of competition between direct dissociation and ring-closure.

compares favorably with the calculated barrier to ring closure on the S_1 surface at 5.72 eV (shown as the solid arrow). The structure of this transition state is shown as an inset to Fig. 2. Fig. 2 also reveals a marked ''inverse'' isotope effect increasing with incidence energy, where DN_3 leads with about twice the efficiency as HN_3 to the *high energy form* of N_3, reaching a maximum of $\sim$10% of the radical channel at about 6 eV. Note that the observed threshold is well below the energetic threshold for spin allowed secondary dissociation to form H + N_2 + $N(^2D)$, which requires 6.2 eV.

Fig. 3 shows the energetics of the relevant pathway for the formation of the cyclic-N_3 species on the S_1 potential surface, extracted from an extensive and highly accurate quantum chemical study of the S_0, S_1, T_1 and S_2 potential energy surfaces. Here, energies (with zero point energy correction) are shown in kcal mol^{-1} along with the optimized structures for local minima and saddle points. Both the barriers to ring closure and to dissociation of the ring closed intermediate are in good agreement with the experimentally observed threshold for the low-translational-energy H-atom producing channel. This leads us to postulate a reasonable mechanism for cyclic-N_3 formation in HN_3 photolysis (Fig. 3); namely, the excitation of HN_3 in this energy range leads to the ring closing transition state with observable efficiency and subsequent formation of the ring-closed intermediate that may then dissociate to the products.

The threshold of the low-translational-energy channel at 5.65 eV is close to the onset of a strong HN_3 absorption that peaks near 210 nm,[52] which we attribute to the $S_0(A') \rightarrow S_2(A')$ absorption. The slow channel production efficiency also shows a leveling off at $\sim$6.1 eV mimicking the energy dependence of the $S_0 \rightarrow S_2$ absorption spectrum. In addition, we observe a rapidly changing value of β near the threshold indicative of the increasing importance of the $S_0 \rightarrow S_2$ absorption. Specifically β's are between -1 and -0.5 for the ''fast channel'', resulting from $S_0(A') \rightarrow S_1(A'')$, but near 0 for the ''slow channel''. It is therefore reasonable to suspect the S_2-state and its subsequent photodynamics as playing an important role in the production of low translational energy N_3 + H. Our *ab-initio* calculations on the S_2-state show a *trans*-minimum with the structure shown in Table 1 and a seam of crossing (conical intersection) between the S_2- and the S_1-state near the *trans*-minimum structure of the S_2 state, also shown in Table 1. Considering the structure of the ground state (also shown in Table 1) excitation to the S_2 Franck–Condon region would result in N–N–N bending and N–N stretching between both N–N-bonds as well as some HNN bending and stretching motion. Molecules excited to S_2 and subsequently transmitted to the S_1-state through the S_2–S_1 seam crossing (conical intersection) would be excited exactly with the proper kind of vibration to provide access to the ring closed transition state of S_1. Thus, the internal conversion to S_1 state will be a dominant process with low excitation energy. Thus excitation to S_2 followed by $S_2 \rightarrow S_1$ internal conversion appears to offer a reasonable explanation for the mechanism of ring closure.

Our *ab initio* calculations also revealed a nearby conical intersection that could transmit S_2 population to S_0. An alternative mechanism for slow atom formation was therefore

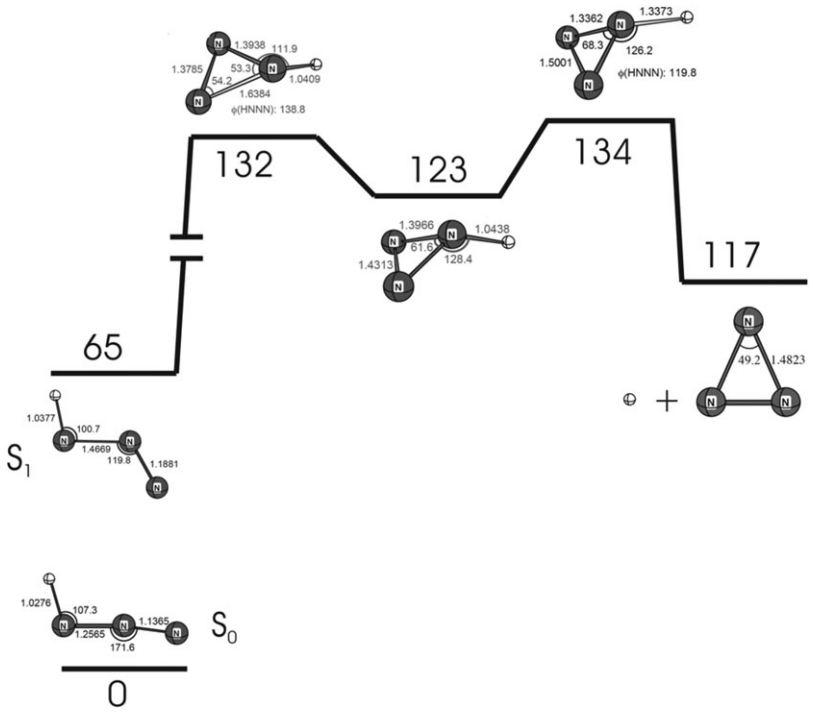

Fig. 3 Postulated cyclization mechanism in HN_3 photolysis. *Ab initio* quantum chemical calculations of isomerization on the S_1 state of HN_3. All energies are shown in kcal mol^{-1} and are corrected for zero-point energy. The near linear N_3 in the S_0 HN_3 is thought to be strongly excited in the bend and N–N stretch leading some reactive flux to the ring-closing barrier and formation of the electronically excited cyclized HN_3. This intermediate may dissociate producing cyclic-N_3.

considered. Here we modeled the fast H-atom production channel as derived from S_0–S_1 excitation and slow atom production as resulting from S_0–S_2 excitation followed by S_2–S_0 internal conversion and statistical decomposition on the S_0 state. We used an RRKM program[53] to model the branching between reactions (1) and (2) on S_0 for both isotopomers, employing reactant and transition state frequencies and energies obtained from our electronic structure calculations. See Table 2. Two major discrepancies with observation arise from this analysis. First, the RRKM analysis predicts a significant (1.7) normal, *i.e.* favoring H-atom production, isotope effect; whereas experiment reveals an isotope effect of similar magnitude but opposite direction, *i.e.* favoring D-atom production. Furthermore, the RRKM predictions cannot reproduce the energy dependence of the isotope effect apparent in Fig. 2. Second, due to the fact that the S_2 absorption is growing rapidly with energy ($\sim 100\times$ stronger than the S_1 absorption at 6 eV), this model predicts that about 90% of all H-atoms would appear in the slow channel (at 6 eV); whereas experiment shows only 5–10%. This analysis strongly suggests that S_2–S_0 internal conversion does not play a role in the production of slow atoms.

In addition to the S_1 ring-closing transition state, the transition state for 1,2 H-atom migration, producing a planar minimum with H attached to the middle N atom, was also found. This barrier is, however, 4.5 kcal mol^{-1} higher in energy than the ring closing barrier. More importantly, in going from the S_0 structure, access to the 1,2 H-atom migration transition state requires a large HNN bending motion, while the ring closure transition state is associated with a large NNN bending motion. The geometrical differences between the S_2 and/or S_1 state global minimum and the

Table 1 Theoretical structure (in Å and °) of the S_2 state and the energy-minimum of the seam crossing (MSX, conical intersection) from S_2 to S_1. The structure of the ground state minimum (S_0) is shown for comparison. All the structures except S_1 ring-closing TS are coplanar ($\phi_{H-N1-N2-N3} = 180.0°$)[a]. Notice how $S_0 \rightarrow S_2 \rightarrow S_1$ leads toward the structure of the S_1 ring closing TS. This is particularly evident for the N_1–N_3 distance and the N_1–N_2–N_3 angle, which are critical to cyclization

	R_{H1-N1}	R_{N1-N2}	R_{N2-N3}	$\Theta_{H-N1-N2}$	$\Theta_{N1-N2-N3}$	R_{N1-N3}
S_0-min	1.028 (1.001)	1.257 (1.251)	1.136 (1.143)	107.3 (108.8)	171.6 (171.4)	2.386 (2.388)
S_2-*trans*-min	(0.992)	(1.301)	(1.286)	(134.9)	(102.2)	(2.013)
S_2-S_1 MSX	(0.992)	(1.302)	(1.287)	(136.7)	(102.1)	(2.014)
S_1-ring closing TS	1.041	1.393	1.378	—	72.5	1.638
S_1-*trans*-min	1.038	1.467	1.188	100.7	119.8	2.301

[a] The geometric parameters in parentheses were optimized at 3 states (S_0, S_1 and S_2 with equal weight) averaged CASSCF(16e/12o)/cc-pVTZ level of theory with σ^*_{N-H} orbital removed from the full valence CASSCF space.

Table 2 Input data for RRKM calculations[a]

	E_0	ν_1	ν_2	ν_3	ν_4	ν_5	ν_6
HN_3	0.0	3386	2189	1313	1155	601	524
$H + N_3$ TS[b]	86.5	—[c]	1645	1320	595	505	95
$NH + N_2$ TS	50.5	3233	2340	—[c]	739	157	120
DN_3	0.0	2475	2181	1172	1003	589	492
$D + N_3$ TS[b]	87.8	—[c]	1645	1320	595	505	95
$ND + N_2$ TS	50.7	2362	2340	—[c]	540	124	116

[a] E_0 (corrected for zero point energy) in kcal mol^{-1}, vibrational frequencies in cm^{-1}. [b] No barrier to dissociation was found. Transition state for N–H(D) bond cleavage was taken as the products H(D) + N_3. [c] Imaginary or zero.

Franck–Condon geometry suggests that the ring-closure transition state is more easily accessible than the 1,2 H-migration transition state and is more likely to be important.

A word regarding the ''inverse'' isotope effect is also in order. An unambiguous interpretation awaits detailed theoretical analysis; however, we speculate that the time available for isomerization to the cyclic structure is approximately double for DN_3 *vs.* HN_3. Remember that isomerization to the cyclic intermediate proceeds in competition with H(D)-atom elimination to form linear N_3. The large negative anisotropy parameter ($\beta \sim -0.7$)[29] for this process indicates sub-picosecond dissociation dynamics. As velocities of the D-atom undergoing direct dissociation will be approximately half that of H-atoms, it is possible that more time is available for the N-atom motion required to close the ring in the case of the heavy departing atom.

In summary, a wavelength dependent study using H-atom Rydberg time-of-flight revealed an energetic threshold for a previously unobserved dissociation pathway in the UV photolysis of hydrazoic acid, exhibiting a threshold that is coincident with a calculated barrier to ring closing on the S_1 (A'') potential energy surface. Theory shows that passage over this barrier leads to a local minimum in the potential, which exhibits an N_3-ring-closed, non-planar structure, which may dissociate to cyclic-N_3 + H. The translational energy release of the newly observed dissociation channel is consistent with the thermodynamics of cyclic-N_3 formation. Through analysis of all experimental observations we propose a detailed photophysical mechanism for cyclic-N_3 formation in HN_3 photolysis. Specifically, we propose that $S_0 \rightarrow S_2$ photo-excitation is followed by $S_2 \rightarrow S_1$ internal conversion through a conical intersection located near the energy minimum of the S_2 state and traversal of the cyclization barrier on S_1 and subsequent N–H bond cleavage. We have analyzed other possible mechanisms of producing ''slow atoms'' and found them inconsistent with experimental observations.

Acknowledgements

AMW acknowledges support from an AFOSR grant No. FA9550-04-1-0057. KM acknowledges support from AFOSR grants No. FA9550-04-1-0080 and FA9550-04-1-0321, as well as a computer-time grant under the DoD High Performance Computing Program.

References

1 L. J. Wang and P. G. Mezey, *J. Phys. Chem. A*, 2005, **109**, 3241–43.
2 D. L. Strout, *J. Phys. Chem. A*, 2004, **108**, 10911–16.
3 L. Y. Bruney, T. M. Bledson and D. L. Strout, *Inorg. Chem.*, 2003, **42**, 8117–20.
4 K. J. Wilson, S. A. Perera, R. J. Bartlett and J. D. Watts, *J. Phys. Chem. A*, 2001, **105**, 7693–99.
5 M. Tobita and R. J. Bartlett, *J. Phys. Chem. A*, 2001, **105**, 4107–13.
6 M. N. Glukhovtsev, H. J. Jiao and P. V. Schleyer, *Inorg. Chem.*, 1996, **35**, 7124–33.
7 A. Vij, J. G. Pavlovich, W. W. Wilson, V. Vij and K. O. Christe, *Angew. Chem., Int. Ed.*, 2002, **41**, 3051–54.
8 K. O. Christe, W. W. Wilson, J. A. Sheehy and J. A. Boatz, *Angew. Chem., Int. Ed.*, 1999, **38**, 2004–09.
9 N. Hansen and A. M. Wodtke, *J. Phys. Chem. A*, 2003, **107**, 10608–14.
10 P. C. Samartzis, J. J. Lin, T. T. Ching, C. Chaudhuri, Y. T. Lee, S. H. Lee and A. M. Wodtke, *J. Chem. Phys.*, 2005, **123**, 051101–1-4.
11 N. Hansen, A. M. Wodtke, S. J. Goncher, J. Robinson, N. Sveum and D. M. Neumark, *J. Chem. Phys.*, 2005, **123**, 104305.
12 A. M. Wodtke, N. Hansen, J. C. Robinson, N. E. Sveum, S. J. Goncher and D. M. Neumark, *Chem. Phys. Lett.*, 2004, **391**, 334–37.
13 N. Hansen, A. M. Wodtke, A. V. Komissarov, K. Morokuma and M. C. Heaven, *J. Chem. Phys.*, 2003, **118**, 10485–93.
14 N. Hansen, A. M. Wodtke, A. V. Komissarov and M. C. Heaven, *Chem. Phys. Lett.*, 2003, **368**, 568–73.
15 M. Bittererova, H. Ostmark and T. Brinck, *J. Chem. Phys.*, 2002, **116**, 9740–48.
16 P. Zhang, K. Morokuma and A. M. Wodtke, *J. Chem. Phys.*, 2005, **122**, 014106–1-11.
17 D. Babikov, B. Kendrick, P. Zhang and K. Morokuma, *J. Chem. Phys.*, 2005, **122**, 044315.
18 D. Babikov, P. Zhang and K. Morokuma, *J. Chem. Phys.*, 2004, **121**, 6743–49.
19 R. J. Barnes, A. Gross, M. Lock and A. Sinha, *J. Phys. Chem. A*, 1997, **101**, 6133–37.
20 M. H. Alexander, H. J. Werner and P. J. Dagdigian, *J. Chem. Phys.*, 1988, **89**, 1388–400.
21 G. Schonnenbeck, H. Biehl, F. Stuhl, U. Meier and V. Staemmler, *J. Chem. Phys.*, 1998, **109**, 2210–19.
22 K. H. Gericke, M. Lock, R. Fasold and F. J. Comes, *J. Chem. Phys.*, 1992, **96**, 422–32.
23 K. H. Gericke, T. Haas, M. Lock, R. Theinl and F. J. Comes, *J. Phys. Chem.*, 1991, **95**, 6104–11.
24 H. H. Nelson and J. R. McDonald, *J. Chem. Phys.*, 1990, **93**, 8777–83.
25 F. Rohrer and F. Stuhl, *J. Chem. Phys.*, 1988, **88**, 4788–99.
26 J. J. Chu, P. Marcus and P. J. Dagdigian, *J. Chem. Phys.*, 1990, **93**, 257–67.
27 J. S. Zhang, K. S. Xu and G. Amaral, *Chem. Phys. Lett.*, 1999, **299**, 285–90.
28 P. A. Cook, S. R. Langford and M. N. R. Ashfold, *Phys. Chem. Chem. Phys.*, 1999, **1**, 45–55.
29 M. Lock, K. H. Gericke and F. J. Comes, *Chem. Phys.*, 1996, **213**, 385–96.
30 T. Haas, K. H. Gericke, C. Maul and F. J. Comes, *Chem. Phys. Lett.*, 1993, **202**, 108–14.
31 K. H. Gericke, M. Lock and F. J. Comes, *Chem. Phys. Lett.*, 1991, **186**, 427–30.
32 K. H. Gericke, R. Theinl and F. J. Comes, *Chem. Phys. Lett.*, 1989, **164**, 605–11.
33 R. Pahnke, S. H. Ashworth and J. M. Brown, *Chem. Phys. Lett.*, 1988, **147**, 179–82.
34 M. Hawley, A. P. Baronavski and H. H. Nelson, *J. Chem. Phys.*, 1993, **99**, 2638–42.
35 R. A. Beaman, T. Nelson, D. S. Richards and D. W. Setser, *J. Phys. Chem.*, 1987, **91**, 6090–92.
36 C. R. Brazier, P. F. Bernath, J. B. Burkholder and C. J. Howard, *J. Chem. Phys.*, 1988, **89**, 1762–67.
37 G. Chambaud and P. Rosmus, *J. Chem. Phys.*, 1992, **96**, 77–89.
38 U. Meier and V. Staemmler, *J. Phys. Chem.*, 1991, **95**, 6111–17.

39 P. A. Cook, P. Jimeno, M. N. R. Ashfold, G. G. Balint-Kurti and R. N. Dixon, *Phys. Chem. Chem. Phys.*, 2002, **4**, 1513–21.
40 W. H. Fang, *J. Phys. Chem. A*, 2000, **104**, 4045–50.
41 L. Schnieder, K. Seekamprahn, J. Borkowski, E. Wrede, K. H. Welge, F. J. Aoiz, L. Banares, M. J. Dmello, V. J. Herrero, V. S. Rabanos and R. E. Wyatt, *Science*, 1995, **269**, 207–10.
42 We will show that this result is consistent with the present results as HN_3 photolysis cannot produce cyclic N_3 until the energy is well above the threshold.
43 L. Schnieder, K. SeekampRahn, E. Wrede and K. H. Welge, *J. Chem. Phys.*, 1997, **107**, 6175–95.
44 L. Schnieder, W. Meier, K. H. Welge, M. N. R. Ashfold and C. M. Western, *J. Chem. Phys.*, 1990, **92**, 7027–37.
45 H. J. Werner and P. J. Knowles, *J. Chem. Phys.*, 1985, **82**, 5053–63.
46 T. H. Dunning, *J. Chem. Phys.*, 1989, **90**, 1007–23.
47 H. J. Werner and P. J. Knowles, *J. Chem. Phys.*, 1988, **89**, 5803–14.
48 P. J. Knowles and H. J. Werner, *Chem. Phys. Lett.*, 1988, **145**, 514–22.
49 E. R. Davidson, *J. Comput. Phys.*, 1975, **17**, 87–94.
50 S. R. Langhoff and E. R. Davidson, *Int. J. Quantum Chem.*, 1974, **8**, 61–72.
51 *MOLPRO* is a package of *ab initio* programs written by H.-J. Werner, P. J. Knowles, M. Schütz, R. Lindh, P. Celani, T. Korona, G. Rauhut, F. R. Manby, R. D. Amos, A. Bernhardsson, A. Berning, D. L. Cooper, M. J. O. Deegan, A. J. Dobbyn, F. Eckert, C. Hampel, G. Hetzer, A. W. Lloyd, S. J. McNicholas, W. Meyer, M. E. Mura, A. Nicklaß, P. Palmieri, R. Pitzer, U. Schumann, H. Stoll, A. J. Stone, R. Tarroni and T. Thorsteinsson.
52 J. R. McDonald, J. W. Rabalais and S. P. McGlynn, *J. Chem. Phys.*, 1970, **52**, 1332.
53 A GENERAL RRKM PROGRAM. L. Zhu, W. L. Hase, 1993. QCPE-644; Available from Quantum Chemistry Program Exchange http://www.qcpe.indiana.edu/.

